RESEARCH ARTICLE

Editorial Process: Submission:01/09/2025 Acceptance:20/10/2026 Published:25/10/2026

Anticancer Activity of Novel Epoxyazadiradione AuNp Complex in TNBC Cells

Jyothsna Unnikrishnan[1], Mangala Hegde[1], Sangeetha Mohan[2,3], Sasidhar B. Somappa[2,3], Ajaikumar B. Kunnumakkara[1]*

Abstract

Background: Triple-negative breast cancer (TNBC) has attracted considerable global research interest due to its complex and poorly understood biology and is characterized by the absence of estrogen receptor (ER), progesterone receptor (PR), and human epidermal growth factor receptor 2 (HER2). **Methods:** Therefore, identifying effective targeted therapeutic approaches for these cells remains a critical challenge. The role of phytochemicals in cancer prevention and treatment is well established and extensively documented. Additionally, gold nanoparticles (AuNps) effectively address several limitations associated with phytochemicals. Therefore, the present study utilized the phytochemical epoxyazadiradione (EAZD) to reduce gold chloride to AuNps, thereby forming the EAZD-AuNP complex. These AuNps, ranging from 10–50 nm in size, can passively target tumor tissue via the enhanced permeability and retention (EPR) effect. Furthermore, the protein corona adsorbed onto the AuNps facilitates cellular uptake via receptor-mediated endocytosis. **Results:** UV–visible spectroscopy, XRD, EDX, and TEM confirmed the formation of EAZD-AuNps. Additionally, FT-IR analysis confirmed the involvement of the carbonyl group of EAZD in the bioreduction of gold chloride. Moreover, in vitro studies using the MTT and colony formation assays revealed an antiproliferative effect of EAZD-AuNps in TNBC cells, with an IC_{50} value of 6 µg/mL. Furthermore, PI-FACS and live/dead assays confirmed that EAZD-AuNps induced a greater extent of cell death than EAZD alone. Western blot analysis further demonstrated that EAZD-AuNps trigger apoptosis through the regulation of cleaved caspase-3 and caspase-9 expression. **Conclusion:** These findings substantiate the anticancer activity of the novel EAZD-AuNP complex. However, additional in vitro and in vivo studies are necessary to further validate its therapeutic potential and should be prioritized.

Keywords: AuNps, phytochemicals, epoxyazadiradione, triple-negative breast cancer, EPR effect

Asian Pac J Cancer Prev, **27 (10)**, 3585-3597

Introduction

Female breast cancer ranks second for frequent cancers around the globe, just behind lung cancer, with an incidence rate of 11.6% [1]. According to immunohistochemistry markers, breast cancer can be categorized into five molecular variants: luminal A, luminal B, *HER2*-enriched, basal-like, and normal-like [2]. The majority of TNBC tumors fall into the basal-like category; however, not all basal-like tumors are TNBC, and vice versa [3]. This highly heterogeneous fetal disease mainly affects premenopausal women of younger age and is estimated to affect 10-20% of breast cancer cases across diverse age populations [4]. These tumors are identified explicitly for the absence of biomarkers (*ER, PR,* and *HER2*). Consequently, TNBC tumors present substantial challenges to the effective implementation of current targeted therapeutic strategies. TNBC frequently metastasizes to essential organs, including the liver, brain, and lungs, and also has a worse prognosis in contrast with other subtypes [5, 6]. Contemporary approaches to the management of TNBC include anthracycline- and cyclophosphamide-based or taxane-based chemotherapy regimens combined with surgery [7, 8]. PI3K/AKT/mTOR inhibitors, epidermal growth factor receptor (EGFR) inhibitors, androgen receptor inhibitors (AR), immune checkpoint inhibitors (ICIs), and targeted agents are under trial for targeted TNBC treatment [9-11]. Nevertheless, a standard systemic therapy for this malignancy remains to be established, highlighting the need for targeted therapies with fewer side effects for TNBC patients.

In modern medical practice, more than 25% of therapeutic agents are derived from natural plants and herbs, with this proportion increasing to approximately 60% among anticancer drugs [12]. In recent years, plant-derived compounds, commonly referred to as

*[1]Cancer Biology Laboratory, Department of Biosciences and Bioengineering, Indian Institute of Technology Guwahati (IITG), Assam 781039, India. [2]Chemical Sciences and Technology Division, CSIR-National Institute for Interdisciplinary Science and Technology (CSIR-NIIST), Thiruvananthapuram, Kerala, India. [3]Academy of Scientific and Innovative Research (AcSIR), Ghaziabad, India. *For Correspondence: kunnumakkara@iitg.ac.in*

phytochemicals, have been extensively investigated worldwide for their therapeutic potential. Paclitaxel, a clinically established FDA-approved chemotherapeutic agent, was initially extracted from the bark of the Pacific yew tree [13]. The primary mechanisms of action of several phytochemicals remain under investigation. Though some studies have shown that their antioxidant properties have played an essential role in cancer therapeutics, as oxidative damage is the leading cause of cancer [14].

EAZD is a limonoid from neem. Neem limonoids possess various therapeutic properties (Figure 1), including antibacterial, anti-inflammatory, antioxidant, and neuroprotective effects [15-18]. The phytochemical EAZD is recognized for its anticancer activity and has been tested in TNBC cells, neuroblastoma, and head and neck squamous cell carcinoma [19-21]. Currently, the efficacy of limonoids is limited by their poor bioavailability and other pharmacokinetic issues [22]. To improve the performance of these compounds, AuNps were introduced as nanocarriers. A substantial body of research has already been established on AuNps as anticancer agents across a wide range of cancer subtypes. In the present work, AuNps were used to target TNBC cells passively via the enhanced permeability and retention (EPR) effect. AuNps within the 10-50 nm size range can evade the rapid renal clearance limit of ~40 kDa, thereby prolonging systemic circulation. [23]. The EPR effect expands tumor vasculatures from 100 nm to 2 µm to maintain excessive growth [24]. Leaky tumor vasculature enables the preferential localization of circulating AuNps in tumor tissue, followed by retention due to poor lymphatic drainage [25].

Furthermore, upon exposure to growth media or plasma proteins, proteins readily adsorb to the surface of AuNps. The protein corona reduces the surface free energy of nanoparticles, also facilitating the cellular uptake of AuNps via receptor-mediated endocytosis (RME) [26, 27]. In this regard, we synthesized AuNps using EAZD as the reducing agent. EAZD-AuNps target the cancer cells passively through the EPR effect. Our in vitro studies revealed antiproliferative, proapoptotic, and anti-clonogenic effects of EAZD-AuNp in TNBC cells.

Materials and Methods

Materials

Gold (III) chloride trihydrate ($HAuCl_4 \cdot 3H_2O$) was sourced from Himedia, India, and dimethyl sulfoxide (DMSO) from Merck (Cat. No. 1.16743.0521, Darmstadt, Germany). Further, Gibco (Cat. No. 25200072) provided trypsin. Sigma-Aldrich (Missouri, USA) supplied 3-(4,5-dimethylthiazol-2-yl)-2,5-diphenyltetrazolium bromide (MTT; Cat. No. M2128) and propidium iodide (PI). SRL Pvt. Ltd., Mumbai, India, supplied crystal violet (Cat. No. 548-62-9). The MDA-MB-231 cells were procured from National Center for Cell Sciences (NCCS), Pune, India. Cell cultures were maintained in DMEM (Gibco™, Life Technologies, NY, USA) enriched with 10% FBS and 1× penicillin-streptomycin, under standard incubation conditions of 37 °C, 5% CO_2, and 95% relative humidity. Sasidhar B. Somappa of the CSIR-National Institute for Interdisciplinary Science and Technology (NIIST) provided EAZD.

Preparation of EAZD-AuNp complex

We prepared a stock solution of 2 mM EAZD in DMSO and dissolved 0.4 mM gold chloride in Milli-Q water. Subsequently, under continuous stirring at 50 °C, 1 ml of EAZD was slowly introduced into 1 ml of the gold chloride solution. The addition of EAZD initially produced white turbidity, which was followed by further heating and stirring for 30 minutes. The solution slowly turned purple as the reduction reaction completed (Figure 2 A-B). Prior to biological studies, the colloidal suspension was centrifuged at 10,000 rpm for 20 minutes, then repeated twice to ensure complete purification of the EAZD-AuNps. Finally, lyophilization yielded the sample as a powder [25, 28].

Characterization of EAZD-AuNp

Characterization of EAZD-AuNps confirmed nanoparticle formation and enabled the morphological feature analysis. UV-visible spectroscopy verified AuNp formation. X-ray diffraction (XRD), selected-area electron diffraction (SAED), and energy-dispersive X-ray spectroscopy (EDX) further validated nanoparticle formation and verified elemental composition. Moreover, Transmission electron microscopy (TEM) revealed morphological characteristics. Fourier transform infrared spectroscopy (FT-IR) elucidated the mechanism of AuNp formation. Anticancer activity of EAZD-AuNps was evaluated using MTT, colony formation, propidium iodide-fluorescence-activated cell sorting (PI-FACS), and live/dead assay. The apoptotic response of MDA-MB-231 cells to EAZD-AuNps was assessed using western blot analysis.

UV-visible spectroscopy



Figure 1. (A) Chemical Structure of the Epoxyazadiradione

The surface plasmon resonance (SPR) studies of AuNps were evaluated using UV-visible spectroscopy over a wavelength range of 400-700 nm. Data acquisition was conducted using a Tecan Infinite 200 PRO multimode microplate reader (Switzerland).

XRD and SAED pattern analysis

XRD is a powerful non-destructive tool for characterizing nanoparticles. XRD analysis was performed using a Rigaku Micromax-007HF diffractometer with Cu $K\alpha_1$ radiation (λ = 1.54060 Å) operated at 40 kV and 40 mA. We used JEM 2100 model from Jeol, Peabody, MA, USA, to perform SAED analysis

EDX analysis

The successful formation of EAZD-AuNps was validated through EDX analysis using a JEOL JEM-2100 instrument (Peabody, MA, USA).

TEM analysis

TEM is a powerful tool for studying objects at the nanometre scale. The morphology and size of AuNps were analyzed by TEM using a JEOL JEM-2100 instrument (Peabody, MA, USA) operated at 200 keV. High-resolution transmission electron microscopy (HR-TEM) imaging revealed the lattice fringes in AuNps, providing insight into interplanar spacing associated with specific crystallographic planes.

FT-IR spectroscopy

FT-IR spectra of EAZD and the EAZD-AuNp complex were recorded separately to elucidate the mechanism of AuNp formation. Measurements acquired over the range of 400-4000 cm^{-1} using a SHIMADZU-8400S spectrophotometer.

MTT assay

Comparative effects of EAZD and EAZD-AuNps treatment on the proliferation of MDA-MB-231 and PSVK-1 cells were evaluated using the MTT assay. In brief, approximately 2000 Cells were seeded into 96-well plates and incubated for 24 h. Then, treated MDA-MB-231 cells with EAZD and EAZD-AuNp at increasing concentrations (1, 2.5, 5, and 10 µg/ml). Likewise, PSVK-1 cells were treated with 20 and 50 µg/ml of the drugs. The MTT assay was performed at 0 and 72 h to assess proliferation. Thereafter, added MTT solution to each well and incubated the plates for 2 hours. Following incubation, an additional 100 µL of DMSO was added after removing the culture medium. Subsequently, we incubated the mixture for 1 hour to ensure complete dissolution of the MTT-formazan product. Then, Absorbance readings were obtained at 570 nm using a microplate reader [25, 28].

Colony-forming assay

Colony-forming potential of cancer cells was assessed by seeding each well of a 6-well plate with 800 cells. After incubation for 1 day, we treated the cells with EAZD and EAZD-AuNp at 5 and 10 µg/ml each. And carefully maintained them for colony formation. Once the colonies formed, they were gently washed with PBS after removing the culture media. Ethanol (100%) was used to fix the cells, after which crystal violet stain was applied. Excess stain was removed by washing the cells with 1× PBS, and the colony-forming images were recorded [28, 29].

PI-FACS assay

The PI-FACS assay is used to analyze the cell death induced by EAZD and EAZD-AuNp. Briefly, MDA-MB-231 cells (5×10^4) were plated in 6-well plates and cultured for 24 hours. After incubation, the cells were treated with 5 and 15 µg/ml of the drugs and incubated for an additional 72 hours. Further, the media containing the dead cells were collected in respective FACS tubes. After three washes with PBS, the cells were subjected to trypsinization for 5 minutes. Finally, collected into designated tubes. Centrifugation was carried out at 4000 rpm for 10 minutes, followed by supernatant removal, and this cycle was repeated twice. The final pellet was resuspended in 5 µL of PI and 495 µL of PBS, followed by analysis of cell death using a BD FACS Celesta™ flow cytometer (Becton, Dickinson, New Jersey, USA) [25, 28].

Live and Dead Assay

Live/dead assay confirmed the anticancer effects of EAZD and EAZD-AuNps on MDA-MB-231 cells. We seeded the cells in a 96-well plate and incubated them for 1 day before treatment with 25 µg/ml of EAZD and EAZD-AuNp. After 72 hours, cells were treated with a staining solution containing 5 µM ethidium homodimer and 5 µM calcein-AM and maintained at room temperature for 15 minutes. Green-colored live cells and red-colored dead cells were examined, and images were recorded using a microscope (Olympus, Japan).

Western blot analysis

Western blotting was employed to examine the apoptotic effects of EAZD-AuNps in MDA-MB-231 cells, with particular focus on the expression of cleaved caspase-3, caspase-9, and caspase-1 to evaluate apoptosis and pyroptosis. Briefly, MDA-MB-231 cells (2.5×10^5) were seeded and maintained at 37 °C for 24 h. Further, the cells were treated with 2, 4, and 8 µg/ml of EAZD-AuNp and cultured for an additional 24h. Cells were harvested, and whole-cell lysates were prepared using a lysis buffer containing 20 mM HEPES, 2 mM EDTA, 250 mM NaCl, 2 µg/mL leupeptin, 2 µg/mL aprotinin, 1 mM PMSF, 1 M DTT, and 0.1% Triton X-100. Protein concentration was quantified using Quick Start™ Bradford 1× dye reagent (Cat. No. 500–0205, Bio-Rad Laboratories, USA). Equal amounts of protein (25 µg per lane) were separated using 12% SDS-PAGE and electrotransferred onto nitrocellulose membranes. Membrane blocking was performed using 5% nonfat dry milk in 1× TBST buffer (24.2 g Tris base, 80 g NaCl, pH 7.6) for 2h at ambient temperature, followed by incubation with primary antibodies at 4 °C. After washing with 1× TBST, membranes were incubated with the corresponding secondary antibodies for 2h. Protein bands were visualized using a ChemiDoc™ XRS+ imaging system (Bio-Rad Laboratories, USA) with Clarity™ Western ECL substrate, and quantified by densitometric analysis using ImageJ software, normalizing to GAPDH.

Statistical analysis

Statistical analysis employed a two-tailed Student's t-test. Data are presented as mean ± standard deviation from at least three independent experiments. Statistical significance was defined as *p < 0.05, **p < 0.01, and **p < 0.001.

Results

Preparation and structural analysis of EAZD-AuNp complex

The anticancer potential of EAZD remains underexplored, although it has been evaluated in TNBC, head and neck squamous cell carcinoma, and neuroblastoma [19, 20, 21]. Limited bioavailability and poor water solubility restrict the potential of phytochemicals as anti-cancer agents [30]. Nanosystems have gained enormous acceptance in the last few decades as targeted drug delivery vehicles, diagnosis, and treatment agents. In the present study, we prepared AuNps by mixing 0.4 mM gold chloride and 2 mM EAZD. After heating and stirring for 30 minutes, the solution turns purple owing to SPR from AuNps [31]. SPR was experimentally confirmed using UV-visible spectroscopy. The UV spectra revealed an absorption peak at 525 nm (Figure 3A). In XRD spectra, fingerprint peaks for AuNps were observed at 38.1°, 44.4°, 64.5°, 77.5°, and 81.7°, attributed to the (111), (200), (220), (311), and (222) FCC planes (Figure 3B). The absence of additional peaks validated the purity of the material. The peak corresponding to the (111) plane is more intense compared to others, which implies the (111) plane is more dominant than other planes in the sample [32]. Moreover, the SAED pattern again confirmed the sample's crystallinity. The observed diffraction rings can be assigned, from inner to outer regions, to the (111), (200), (220), (311), and (222) reflections characteristic of FCC gold [33]. Quantitative verification of the presence of EAZD and the AuNps was performed using EDX spectra. EDX showed peaks for Au, C, and O; the highly intense peak at 8 keV corresponds to Cu and originates from the copper grid. The peak around ~2 keV is characteristic of metallic AuNps and is consistent with previous studies [25, 34]. Carbon and oxygen peaks might have originated from the EAZD bound to the surface of the AuNps (Figure 3C). TEM was employed to analyze the size and morphology of the nanoparticles, as these parameters are critical for biological applications. TEM images revealed that AuNps were hexagonal. Though the particles are poly-dispersed, they are in the 10-50 nm size range, a typical size for cellular administration. Hexagonal-shaped AuNps have been shown to exhibit effective anti-cancer properties in breast and brain cancer cells [35, 36]. Lattice spacing calculated from the TEM image was 0.204nm, corresponding to the (200) plane of AuNps (Figure 3D-F).

FT-IR spectra of EAZD showed two carbonyl peaks at 1735 cm^{-1} and 1666 cm^{-1}. In AuNps, one carbonyl peak shifted to 1658 cm^{-1}, and the hydroxyl group appeared at 3387 cm^{-1}. After the bioreduction, the shift in the peak at 1666 cm^{-1} towards lower frequency (1658 cm^{-1}) indicates the involvement of the carbonyl moiety in the bioreduction. The carbonyl group might have been involved in a reduction and stabilization mechanism of AuNps (Figure 4) [28, 37, 38].

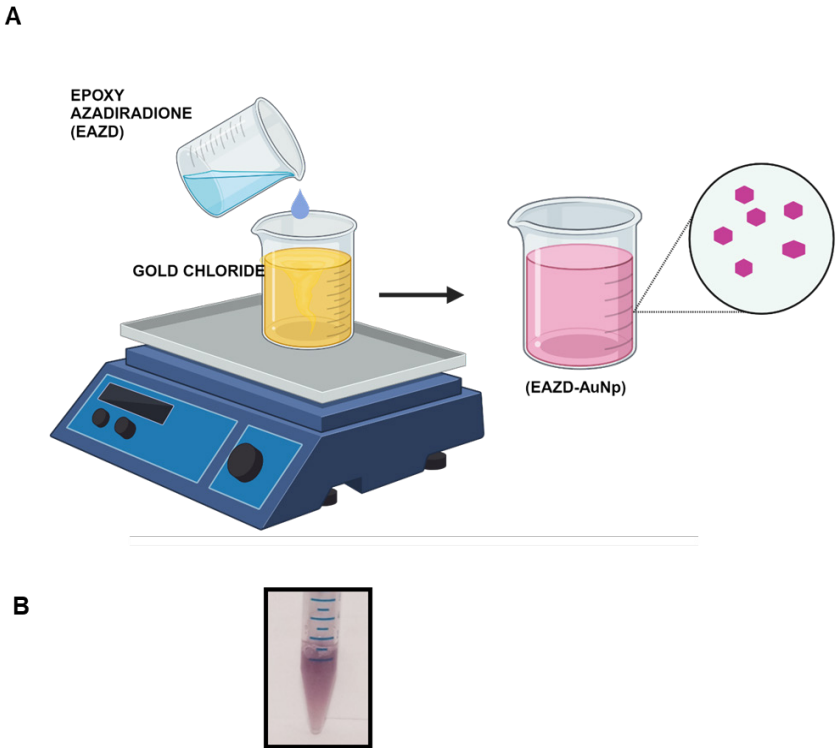


Figure 2. Synthesis of EAZD-AuNp: (A) A schematic model of EAZD-AuNp preparation. EAZD was mixed with gold chloride under continuous magnetic stirring (50 °C). (B) After the bioreduction of gold chloride, the solution turns purple.

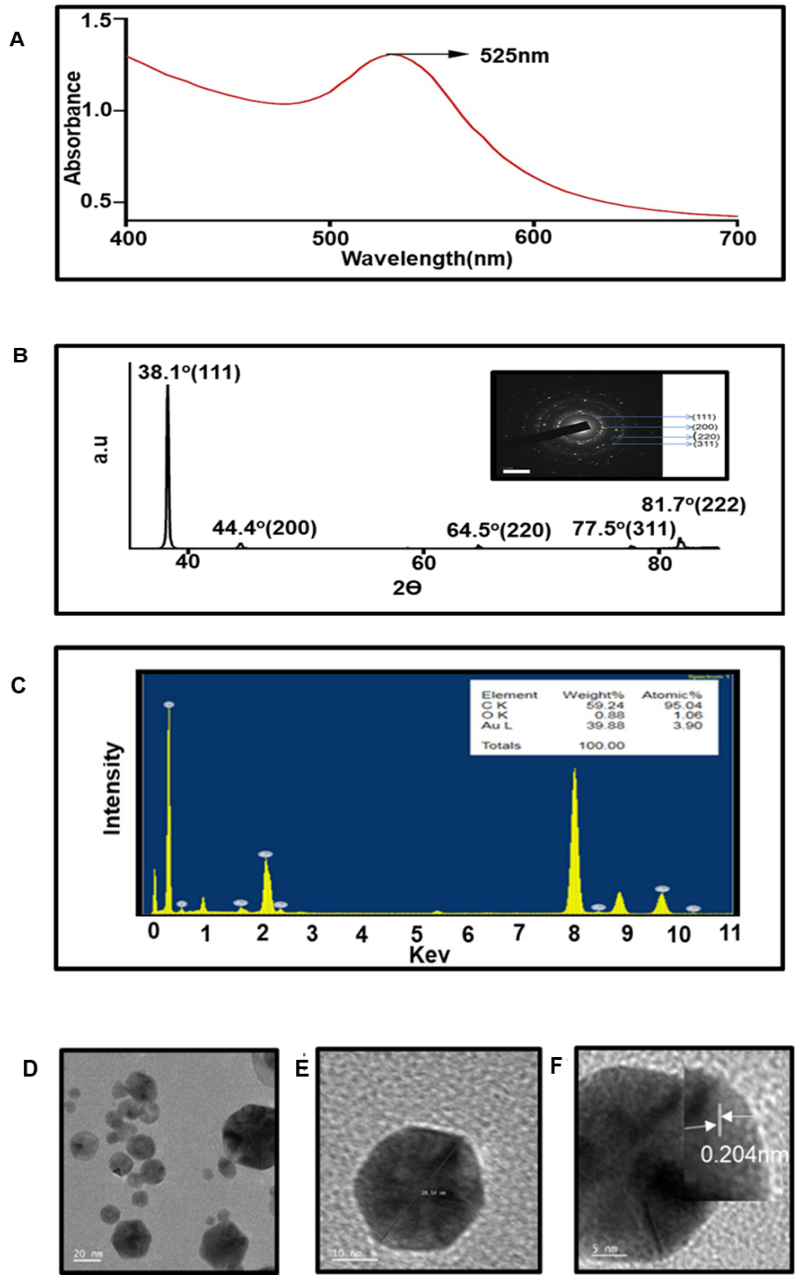


Figure 3. Structural Analysis of EAZD-AuNp: (A) UV-Vis spectra analysis from 400-700 nm, displayed an absorption peak at 525nm; (B) XRD data confirmed the formation of AuNp, and showed five finger-print peaks of FCC gold. The SAED pattern showed diffraction rings corresponding to the crystal planes. (C) EDX data further verified the presence gold qualitatively and quantitatively, showing the peaks for Au, C, and O. (D)-(F) TEM images revealed the hexagonal structure of AuNps at 20 nm and 10 nm scale, and the HR-TEM image expressed the fringe spacing in the crystalline nanoparticles.

Anti-proliferation study of EAZD and EAZD-AuNp using MTT and colony formation assay.

Following the structural analysis, we moved to antiproliferative studies of EAZD-AuNp. Although bare EAZD did not show any effect up to 10 µg/ml, EAZD-AuNp showed a significant reduction in proliferation with increasing drug concentration. EAZD-AuNp showed 26% reduction at 1 µg/ml, 39% greater reduction at 5 µg/ml, and 89% reduction at 10 µg/ml compared to the control. The IC50 for EAZD-AuNp was 6 µg/ml. Further, the toxicity of EAZD and EAZD-AuNps was analyzed in the PSVK-1 normal skin epithelial cell line. Both EAZD and its nanoparticle counterpart exhibited minimal toxicity at 20 µg/ml. However, at 50 µg/ml, EAZD-AuNps displayed slight toxicity (Figure 5 A1-A2).

The clonogenic potential is crucial for cancer cells, as it measures the ability of a single cell to survive and reproduce to form colonies. It is noteworthy that EAZD and EAZD-AuNp have significantly reduced proliferation compared to the control. While EAZD-AuNp-treated cells barely survived for colony formation. Treatment with EAZD-AuNps resulted in enhanced reduction in clonogenic potential at 5 µg/ml and 10 µg/ml, respectively, relative to bare EAZD-treated cells (Figure 5 B-C).

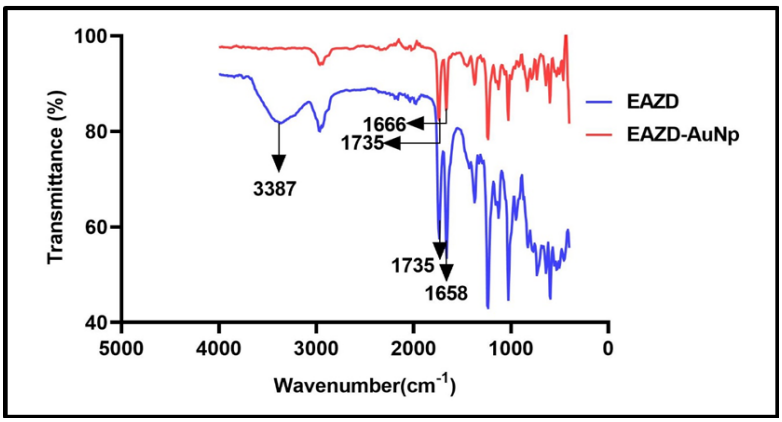


Figure 4. FT-IR Spectra of EAZD and EAZD-AuNp: FT-IR analysis of EAZD-AuNp revealed a peak shift at 1658cm-1 (CO group) from 1666cm-1 in EAZD

Cell viability analysis of EAZD and EAZD-AuNp

PI-FACS analysis was performed to assess TNBC cell viability. EAZD induced 13% and 44% cell death, while EAZD-AuNp-treated wells showed 27% and 61% cell death at 5µg/ml and 15 µg/ml, respectively. These studies revealed that EAZD-AuNp induced 13% and 17% greater cell death at 5 µg/ml and 15 µg/ml, compared to its phytochemical counterpart. A live/dead assay further confirmed the effect of EAZD-AuNp on TNBC cell survival. EAZD-AuNp induced more cell death than EAZD at 10 µg/ml. Altogether, EAZD-AuNp displayed a more pronounced cytotoxic effect than EAZD and the control (Figure 6A-I).

Elucidation of the mechanism of action of EAZD-AuNps in MDA-MB-231 cells

The effect of EAZD-AuNps on apoptosis-associated proteins was evaluated by Western blot analysis, focusing on cleaved caspase-3, caspase-9, and caspase-1. Treatment of MDA-MB-231 cells with increasing concentrations of EAZD-AuNps (2, 4, and 8 µg/mL) induced the expression of these apoptotic markers (Figure 7A). The levels of cleaved caspase-9 and cleaved caspase-3 were elevated at 2 and 4 µg/mL, indicating activation of the intrinsic (mitochondrial-mediated) apoptotic pathway (Figure 7B-C). At the higher concentration (8 µg/mL), a modest reduction in the levels of cleaved caspase-3 and caspase-9 was observed compared to 2 and 4 µg/mL; however, their expression remained elevated relative to the untreated control. This trend suggests that EAZD-AuNps induce apoptosis in a dose-dependent manner up to an optimal concentration, beyond which the response slightly declines, potentially due to cellular stress dynamics or feedback regulation. In contrast, no detectable expression of cleaved caspase-1 was observed, suggesting that the pyroptotic pathway was not activated under these conditions (Figure 7A).

Discussion

TNBC tumors are well-identified for their higher nuclear grade, high mitotic activity, and poor prognosis [39, 40]. Effectively managing these highly heterogeneous tumors within the constraints of current therapeutic approaches remains a significant challenge. However, several combinational therapies are under clinical trial for TNBC (phase I/II), while targeted systemic therapies remain behind the curtain [5, 41-43]. Approximately 5,000 phytochemicals have been identified to date, many of which exhibit significant anticancer and antioxidant properties [44-46]. EAZD represents a promising phytochemical that remains insufficiently investigated for its potential health benefits, despite documented evidence of its anticancer, anti-inflammatory, and antidiabetic properties [47-49]. Nevertheless, the therapeutic efficacy of phytochemicals is frequently constrained by limited bioavailability, rapid systemic clearance, and the emergence of resistance [50, 51]. It is evident that nanotechnology tools can efficiently overcome the limitations of phytochemicals [52]. The nanoparticle size is a critical factor in the EPR effect; the ideal size is 10-100 nm for efficient passive targeting [53-55] (Figure 8A). In addition, the protein corona adsorbed on the nanoparticles facilitates internalization via RME, leading to cell death (Figure 8B) [26]. In effect, EAZD-AuNp of 10-50 nm could target TNBC cells successfully.

In the current study, AuNps were prepared using EAZD as a precursor. The phyto-nano complex was analyzed for anti-cancer properties in TNBC cells (Figure 8C). AuNps formation was primarily as reflected by the shift in suspension color from yellow to purple [25, 28]. The colour change was attributed to the localized SPR of AuNps [56]. UV–visible spectroscopy was employed to verify the SPR peak of AuNps, with an absorption peak at 525 nm, in agreement with other reports [57, 58]. Further, the XRD spectrum verified characteristic AuNp peaks at 38.1°, 44.4°, 64.5°, 77.5°, and 81.7°, corresponding to the (111), (200), (220), (311), and (222) planes, respectively. The SAED pattern displayed diffraction rings from the interior to the exterior, indexed as (111), (200), (220), and (311), corresponding to the crystal planes. SAED pattern with bright circular rings also confirms the polycrystalline nature of the AuNps [59]. EDX further validated the formation of AuNps, showing peaks for C, O, and Au. A peak around 2 keV was a clear indication of the presence of crystalline AuNps in the sample; the carbon and oxygen

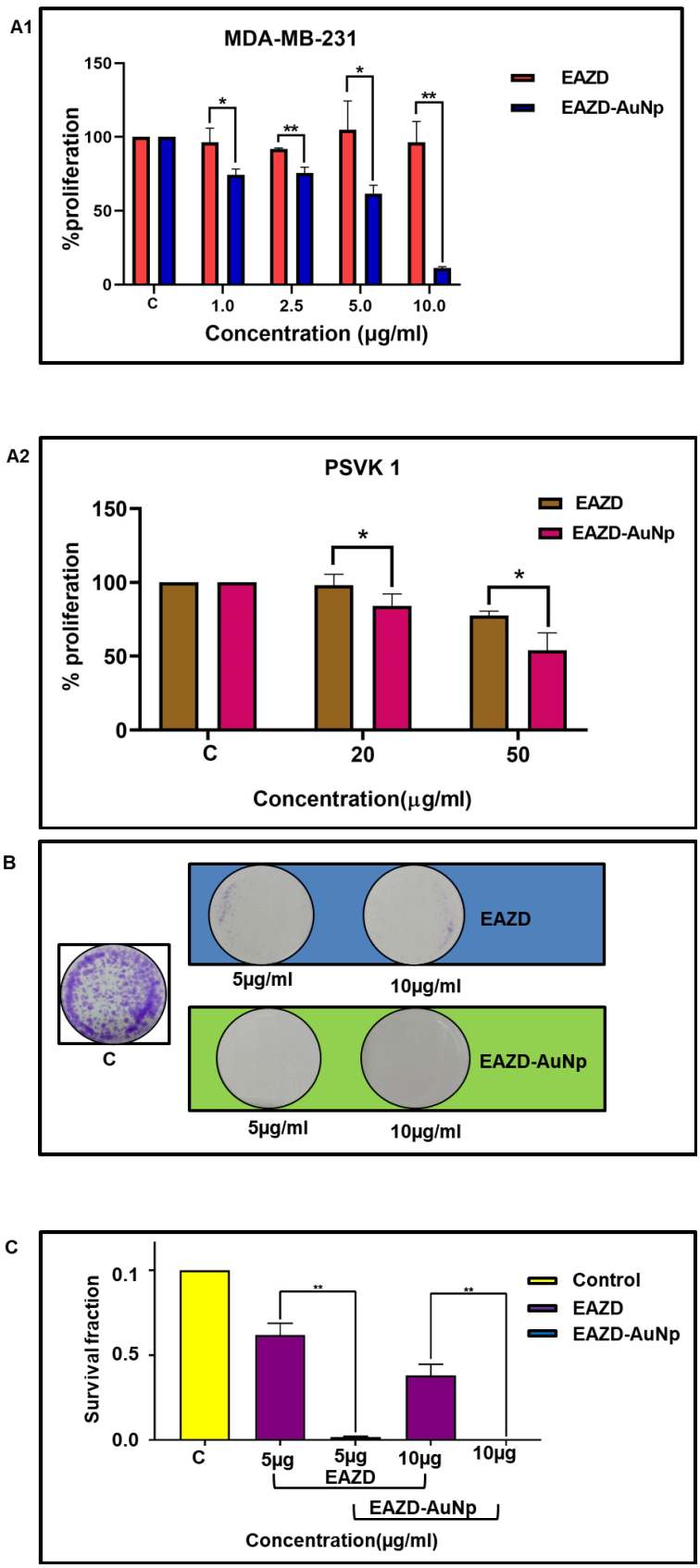


Figure 5. Antiproliferative and Anti-Clonogenic Effect on MDA-MB-231 Cells. (A1) and (A2) MTT assay: Antiproliferative aspects of EAZD and EAZD-AuNp on MDA-MB-231 and PSVK-1 cells, respectively. A t-test for the MTT assay was performed in triplicate; the p-values were 0.02 (*), 0.01 (**), 0.03 (*), and 0.006 (**) for 1, 2.5, 5, and 10 µg/ml, respectively. Similarly, PSVK-1 cells were compared across triplicates, with p-values of 0.02 (*) for 20 µg/ml and 0.03 (*) for 50 µg/ml. (B) Colony formation assay: Verified the decrease in clonogenic potential of the cancer cells with the addition of EAZD and EAZD-AuNp at two different concentrations. (C) Quantitative analysis of colony formation assay: Studied the survival fraction of cells upon the treatment of EAZD and EAZD-AuNp (ImageJ software); A t-test for colony analysis, also carried out in triplicate, yielded p-values of 0.004 (**) for 5 µg/ml and 0.009 (**) for 10 µg/ml. C: control

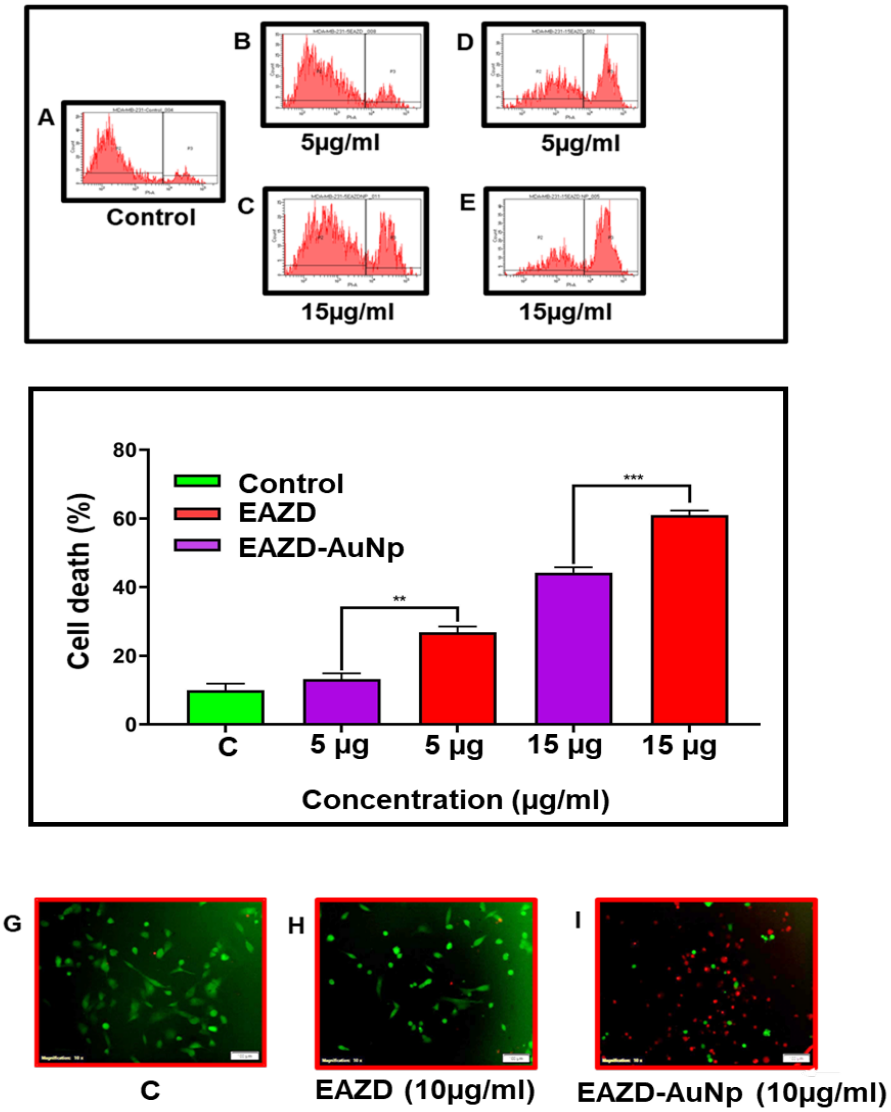


Figure 6. *In vitro* Cell Death Analysis of EAZD and EAZD-AuNp in MDA-MB-231 cells. (A-D) PI-FACS assay: PI-FACS analyzed the cell death induced by 5 µg/ml and 15 µg/ml of the drugs for 3 days. Quantification of PI-FACS assay verified that EAZD –AuNp induced more cell death than EAZD alone; (E-G) Live and dead assay: cells were treated with 10 µg/ml of the drugs and verified the cell death induced. Images were recorded at 10X magnification and 100µm scale. The p-values for PI-FACS measurements are 0.008 (**) for 5 µg/ml and 0.00018 (***) for 15 µg/ml, compared for triplicates. C: control

peaks were also attributed to the phytochemicals [60, 61]. The shape and size of the nanoparticle played an essential role in their biological activities [62, 63]. TEM revealed that EAZD-AuNps were hexagonally shaped. Particles were below 50 nm in size, even though they were polydispersed. Additionally, FT-IR spectra showed a shift in the carbonyl peak to a lower frequency (1658 cm^{-1}) after bioreduction of $HAuCl^4$ with EAZD, indicating the involvement of the carbonyl group in the bioreduction.

Further, to evaluate the anticancer potential of the phyto-nano complex, we analyzed the cytotoxicity and cell viability of EAZD-AuNp in MDA-MB-231 breast cancer cells. MTT assay showed a significant reduction in proliferation compared to EAZD. Even at 10 µg/ml, EAZD-AuNp induced 89% reduction in proliferation, with a very low IC50 of 6 µg/ml. Also verified the non-toxicity of EAZD-AuNp in PSVK-1 normal skin epithelial cells. Moreover, EAZD-AuNp dramatically reduced the clonogenic potential of MDA-MB-231 cells; no colonies survived in the drug-treated well (10 µg/ml). PI-FACS results showed 61% cell death in EAZD-AuNp-treated cells (15 µg/ml). The cytotoxic potential of EAZD-AuNps in MDA-MB-231 cells was further supported by live-dead assay results. Western blot analysis elucidated the mechanism of action of EAZD-AuNps, revealing upregulation of cleaved caspase-3 and caspase-9 expression, a clear indication of mitochondria-mediated apoptosis [64]. However, EAZD-AuNps did not induce caspase-1 cleavage, suggesting that the treatment promotes mitochondria-mediated apoptosis without activating pyroptotic pathways [65]. Collectively, these findings suggest that hexagonal EAZD-AuNps exhibit significant in vitro anticancer activity. Nevertheless, their potential as a therapeutic candidate warrants further validation through comprehensive in vivo studies to establish clinical relevance.

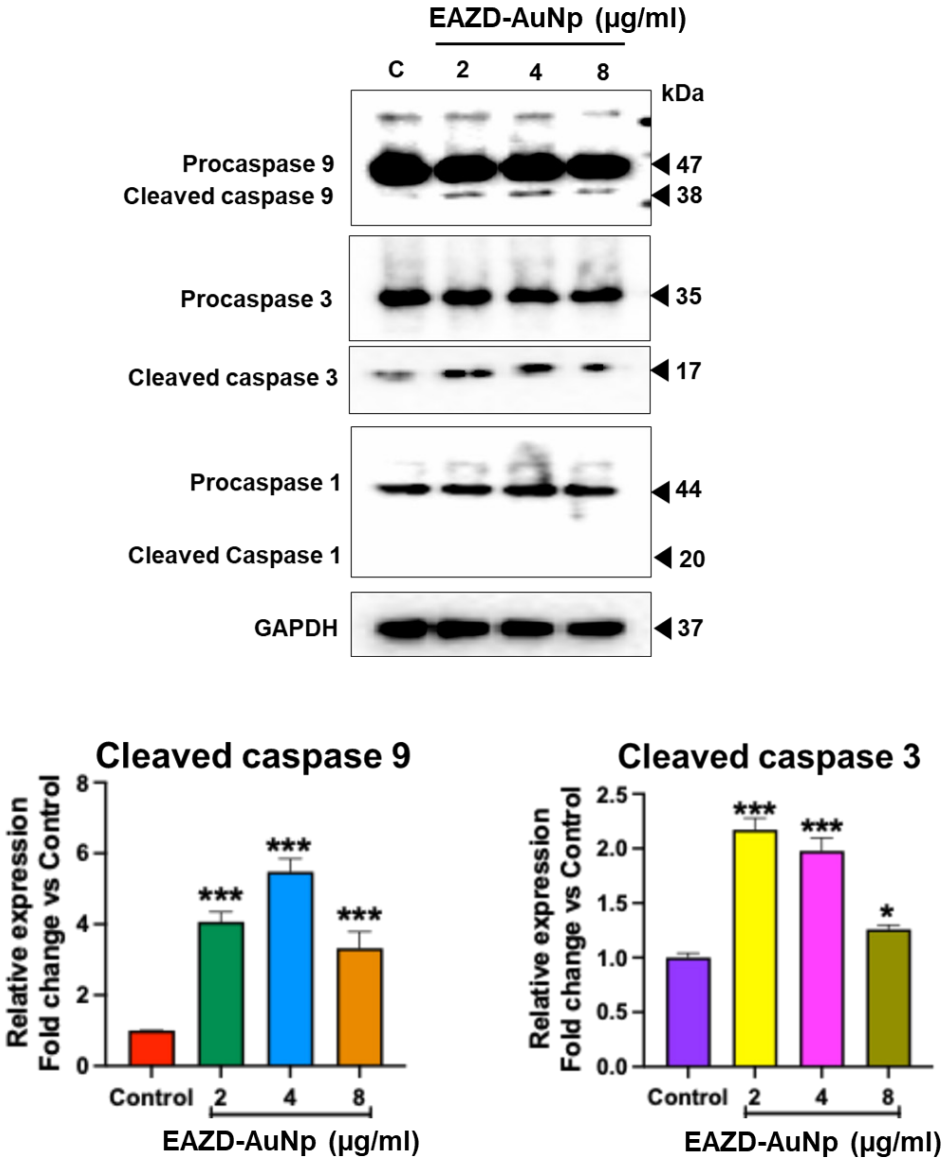


Figure 7. (A) Effect of EAZD on apoptotic proteins. Expression of cleaved caspase 3 and 9 in MDA-MB-231 cells after treatment with EAZD-AuNp at 2, 4, and 8 µg/ml. (B) and C) relative expression of cleaved caspase-9 and caspase-3. Cell lysate was prepared after 24h of treatment with EAZD-AuNp. GAPDH was taken as the housekeeping gene. Statistical significance was analyzed using a t-test, comparing all EAZD-AuNp-treated groups with the control. P-values obtained for cleaved caspase-9 were 0.0028 (**), 0.0022(**), and 0.0133(*) for 2, 4, and 8 µg/ml in the order. Similarly, P-values for cleaved caspase-3 were 0.0037(**), 0.0056(**), 0.0317(*) for 2, 4, and 8 µg/ml each C: control

Conclusion and future work

This study demonstrates that EAZD-AuNp significantly enhances the anticancer efficacy of the parent phytochemical against TNBC cells, primarily by reducing cell proliferation and promoting cell death. The improved biological activity is likely attributable to nanoscale size, enhanced cellular internalization, and synergistic effects between EAZD and AuNps. The results underscore the potential of EAZD-AuNps as an effective system for phytochemical-based nanotherapeutic strategies.

Future investigations should focus on in vivo validation, including biodistribution, pharmacokinetics, toxicity profiling, and therapeutic efficacy, to establish clinical translational potential. Additionally, studies exploring the molecular pathways underlying induced cytotoxicity would strengthen the therapeutic relevance of this nanocomplex.

Author Contribution Statement

JU: Performed experiments, data curation, Formal analysis, investigation, validation, visualization, and original draft preparation. MH: Formal analysis, data curation, overall review, and editing. SM and SH: Extracted the compound validation. ABK: Conceptualization, Supervision, proof reading, Project administration, Funding acquisition.

Acknowledgements

Mangala Hegde acknowledges a research associate fellowship (DBT-RA/2023/July/NE/4835) from the

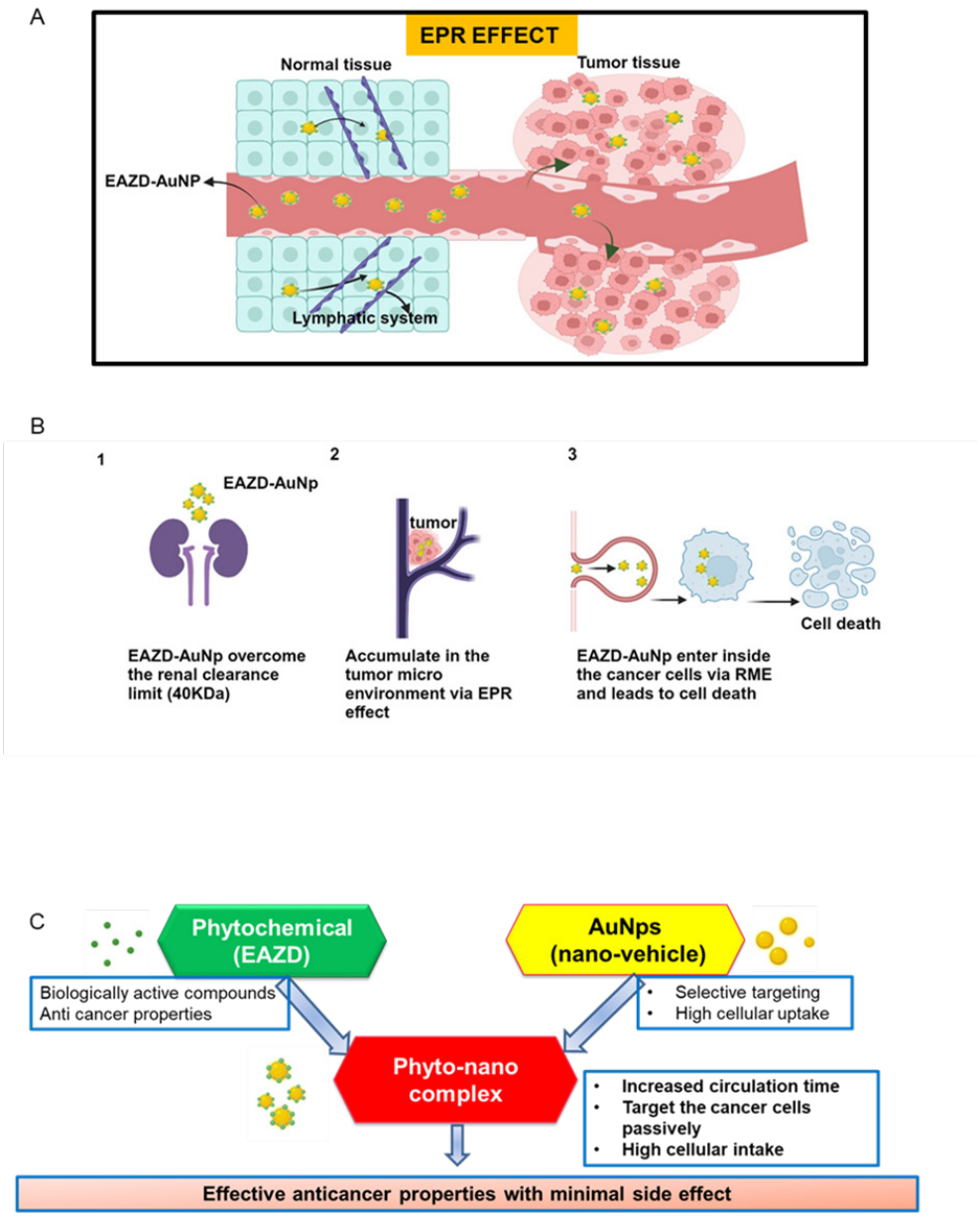


Figure 8. (A) Schematic representation of EPR effect (B) Schematic for the proposed mechanism of internalization of EAZD-AuNp in TNBC cells. (C) Pictorial representation of the peculiar properties of novel phyto-nano complex

Department of Biotechnology (DBT), Government of India. We acknowledge the assistance from CIF (IIT Guwahati). Jyothsna acknowledges MHRD, Government of India, for the fellowship. We thank Dr. Archana M. Nair (Department of Civil Engineering, IIT Guwahati) for her help and support.

Approval by scientific body/thesis

This work is a part of the PhD thesis work of the author Jyothsna Unnikrishnan.

Data availability

Data is available on request

The figures in this paper were created using Biorender software (BioRender.com). Authors acknowledge the use of artificial intelligence (ChatGPT) for improving language and readability.

Funding

This project was supported by the BT/556/NE/U-Excel/2016 grant awarded to ABK by the Department of Biotechnology (DBT), Government of India.

Ethical approval

Ethical approval was not sought for the present study because this article does not contain any studies with human or animal subjects

Conflict of Interest

The authors declare that they have no known competing financial interests or personal relationships that could have influenced the work in this paper.

Abbreviations

TNBC: Triple-negative breast cancer; Au: Gold; *HER2*: Human epidermal growth factor 2; DMSO:

Dimethyl sulfoxide; DMEM: Dulbecco's Modified Eagle Medium; FBS: Fetal Bovine Serum; EAZD: Epoxy azadiradione; EAZD-AuNp: Epoxyazadiradione - gold nanoparticles; EGFR: Epidermal growth factor receptor; AR: Androgen receptor; ICIs: Immune checkpoint receptor; RME: Receptor-mediated endocytosis, EPR: Enhanced permeability and retention effect; ER: Estrogen receptor; PR: Progesterone receptor; SPR: surface plasmon resonance; FTIR: Fourier-transform infrared spectroscopy; MTT: 3-(4,5-dimethylthiazol-2-yl)-2,5-diphenyltetrazolium bromide; PBS: Phosphate buffer saline; PI-FACS: Propidium iodide- fluorescence-activated cell Sorting; SAED: Selective area diffraction pattern; TEM: Transmission electron microscopy; XRD: X-Ray diffraction spectroscopy; EDX: Energy dispersive X-ray analysis.

References

1. Bray F, Laversanne M, Sung H, Ferlay J, Siegel RL, Soerjomataram I, et al. Global cancer statistics 2022: Globocan estimates of incidence and mortality worldwide for 36 cancers in 185 countries. CA Cancer J Clin. 2024;74(3):229-63. https://doi.org/10.3322/caac.21834.
2. Vallejos CS, Gomez HL, Cruz WR, Pinto JA, Dyer RR, Velarde R, et al. Breast cancer classification according to immunohistochemistry markers: Subtypes and association with clinicopathologic variables in a peruvian hospital database. Clin Breast Cancer. 2010;10(4):294-300. https://doi.org/10.3816/CBC.2010.n.038.
3. Prat A, Adamo B, Cheang MC, Anders CK, Carey LA, Perou CM. Molecular characterization of basal-like and non-basal-like triple-negative breast cancer. Oncologist. 2013;18(2):123-33. https://doi.org/10.1634/theoncologist.2012-0397.
4. Otvos L, Jr., Kovalszky I, Riolfi M, Ferla R, Olah J, Sztodola A, et al. Efficacy of a leptin receptor antagonist peptide in a mouse model of triple-negative breast cancer. Eur J Cancer. 2011;47(10):1578-84. https://doi.org/10.1016/j.ejca.2011.01.018.
5. Nakhjavani M, Samarasinghe RM, Shigdar S. Triple-negative breast cancer brain metastasis: An update on druggable targets, current clinical trials, and future treatment options. Drug Discov Today. 2022;27(5):1298-314. https://doi.org/10.1016/j.drudis.2022.01.010.
6. Yao Y, Chu Y, Xu B, Hu Q, Song Q. Risk factors for distant metastasis of patients with primary triple-negative breast cancer. Biosci Rep. 2019;39(6). https://doi.org/10.1042/BSR20190288.
7. Korde LA, Somerfield MR, Carey LA, Crews JR, Denduluri N, Hwang ES, et al. Neoadjuvant chemotherapy, endocrine therapy, and targeted therapy for breast cancer: Asco guideline. J Clin Oncol. 2021;39(13):1485-505. https://doi.org/10.1200/JCO.20.03399.
8. Narui K, Ishikawa T, Shimizu D, Yamada A, Tanabe M, Sasaki T, et al. Anthracycline could be essential for triple-negative breast cancer: A randomised phase ii study by the kanagawa breast oncology group (kbog) 1101. Breast. 2019;47:1-9. https://doi.org/10.1016/j.breast.2019.06.003.
9. Khan MA, Jain VK, Rizwanullah M, Ahmad J, Jain K. Pi3k/akt/mtor pathway inhibitors in triple-negative breast cancer: A review on drug discovery and future challenges. Drug Discovery Today. 2019;24(11):2181-91. https://doi.org/10.1016/j.drudis.2019.09.001.
10. Corkery B, Crown J, Clynes M, O'Donovan N. Epidermal growth factor receptor as a potential therapeutic target in triple-negative breast cancer. Ann Oncol. 2009;20(5):862-7. https://doi.org/10.1093/annonc/mdn710.
11. Bou Zerdan M, Ghorayeb T, Saliba F, Allam S, Bou Zerdan M, Yaghi M, et al. Triple negative breast cancer: Updates on classification and treatment in 2021. Cancers (Basel). 2022;14(5):1253. https://doi.org/10.3390/cancers14051253.
12. Najmi A, Javed SA, Al Bratty M, Alhazmi HA. Modern approaches in the discovery and development of plant-based natural products and their analogues as potential therapeutic agents. Molecules. 2022;27(2):349. https://doi.org/10.3390/molecules27020349.
13. Vaishampayan U, Parchment RE, Jasti BR, Hussain M. Taxanes: An overview of the pharmacokinetics and pharmacodynamics. Urology. 1999;54(6A Suppl):22-9. https://doi.org/10.1016/s0090-4295(99)00451-3.
14. Prakash D, Gupta K. The antioxidant phytochemicals of nutraceutical importance. The Open Nutraceuticals Journal. 2009;2(1). https://doi.org/10.2174/1876396000902010020.
15. Ghonmode WN, Balsaraf OD, Tambe VH, Saujanya K, Patil AK, Kakde DD. Comparison of the antibacterial efficiency of neem leaf extracts, grape seed extracts and 3% sodium hypochlorite against e. Feacalis–an in vitro study. J Int Oral Health. 2013;5(6):61.
16. Ilango K, Maharajan G, Narasimhan S. Anti-nociceptive and anti-inflammatory activities of azadirachta indica fruit skin extract and its isolated constituent azadiradione. Nat Prod Res. 2013;27(16):1463-7. https://doi.org/10.1080/14786419.2012.717288.
17. Ghimeray AK, Jin C-W, Ghimire BK, Cho DH. Antioxidant activity and quantitative estimation of azadirachtin and nimbin in azadirachta indica a. Juss grown in foothills of nepal. Afr J Biotechnol. 2009;8(13).
18. Abdel Moneim AE, Othman MS, Aref AM. Azadirachta indica attenuates cisplatin-induced nephrotoxicity and oxidative stress. Biomed Res Int. 2014;2014:647131. https://doi.org/10.1155/2014/647131.
19. Rai V, Aggarwal SK, Verma SS, Awasthee N, Dhasmana A, Aggarwal S, et al. Epoxyazadiradione exhibit activities in head and neck squamous cell carcinoma by targeting multiple pathways. Apoptosis. 2020;25(9-10):763-82. https://doi.org/10.1007/s10495-020-01633-1.
20. Kumar D, Haldar S, Gorain M, Kumar S, Mulani FA, Yadav AS, et al. Epoxyazadiradione suppresses breast tumor growth through mitochondrial depolarization and caspase-dependent apoptosis by targeting pi3k/akt pathway. BMC cancer. 2018;18(1):1-17. https://doi.org/10.1186/s12885-017-3876-2.
21. Chandel S, Bhattacharya A, Gautam A, Zeng W, Alka O, Sachsenberg T, et al. Investigation of the anti-cancer potential of epoxyazadiradione in neuroblastoma: Experimental assays and molecular analysis. J Biomol Struct Dyn. 2024;42(21):11377-95. https://doi.org/10.1080/07391102.2023.2262593.
22. Roy A, Datta S, Bhatia KS, Jha P, Prasad R. Role of plant derived bioactive compounds against cancer. S Afr J Bot. 2021.
23. Iyer AK, Khaled G, Fang J, Maeda H. Exploiting the enhanced permeability and retention effect for tumor targeting. Drug Discov Today. 2006;11(17-18):812-8. https://doi.org/10.1016/j.drudis.2006.07.005.
24. Kalyane D, Raval N, Maheshwari R, Tambe V, Kalia K, Tekade RK. Employment of enhanced permeability and retention effect (epr): Nanoparticle-based precision tools for targeting of therapeutic and diagnostic agent in cancer. Mater Sci Eng A. 2019;98:1252-76. https://doi.org/10.1016/j.msec.2019.01.066.

25. Unnikrishnan J, Hegde M, Girisa S, Satpati P, Kunnumakkara AB. Ellagic acid-gold nanoparticle complex as anticancer agent in triple-negative breast cancer cells. Nano Life. 2024;14(02):2450003. https://doi.org/10.1142/S179398442450003X.
26. Vácha R, Martinez-Veracoechea FJ, Frenkel D. Receptor-mediated endocytosis of nanoparticles of various shapes. Nano letters. 2011;11(12):5391-5. https://doi.org/10.1021/nl2030213.
27. Cedervall T, Lynch I, Foy M, Berggard T, Donnelly SC, Cagney G, et al. Detailed identification of plasma proteins adsorbed on copolymer nanoparticles. Angew Chem Int Ed Engl. 2007;46(30):5754-6. https://doi.org/10.1002/anie.200700465.
28. Jyothsna U, Mangala H, Aviral K, Sosmitha G, Priyadarshi S, Ajaikumar BK. Biogenic synthesis and characterization of ethyl ferulate gold nanoparticle and its efficacy against triple-negative breast cancer cells. Curr Nanomed. 2025;15(1):80-94. https://doi.org/10.2174/0124681873280022240130062923.
29. Bordoloi D, Banik K, Vikkurthi R, Thakur KK, Padmavathi G, Sailo BL, et al. Inflection of akt/mtor/stat-3 cascade in tnf-alpha induced protein 8 mediated human lung carcinogenesis. Life Sci. 2020;262:118475. https://doi.org/10.1016/j.lfs.2020.118475.
30. Bansal SS, Goel M, Aqil F, Vadhanam MV, Gupta RC. Advanced drug delivery systems of curcumin for cancer chemoprevention. Cancer Prev Res (Phila). 2011;4(8):1158-71. https://doi.org/10.1158/1940-6207.CAPR-10-0006.
31. Kelly KL, Coronado E, Zhao LL, Schatz GC. The optical properties of metal nanoparticles: The influence of size, shape, and dielectric environment. ACS Publications; 2003. p. 668-77.
32. Philip D. Honey mediated green synthesis of gold nanoparticles. Spectrochim Acta A Mol Biomol Spectrosc. 2009;73(4):650-3. https://doi.org/10.1016/j.saa.2009.03.007.
33. Sujitha MV, Kannan S. Green synthesis of gold nanoparticles using citrus fruits (citrus limon, citrus reticulata and citrus sinensis) aqueous extract and its characterization. Spectrochim Acta A Mol Biomol Spectrosc. 2013;102:15-23. https://doi.org/10.1016/j.saa.2012.09.042.
34. Fayaz AM, Girilal M, Mahdy SA, Somsundar S, Venkatesan R, Kalaichelvan P. Vancomycin bound biogenic gold nanoparticles: A different perspective for development of anti vrsa agents. Process biochemistry. 2011;46(3):636-41. https://doi.org/10.1016/j.procbio.2010.11.001.
35. Mukherjee S, Sushma V, Patra S, Barui AK, Bhadra MP, Sreedhar B, et al. Green chemistry approach for the synthesis and stabilization of biocompatible gold nanoparticles and their potential applications in cancer therapy. Nanotechnology. 2012;23(45):455103. https://doi.org/10.1088/0957-4484/23/45/455103.
36. Ohadi M, Forootanfar H, Dehghannoudeh G, Eslaminejad T, Ameri A, Shakibaie M, et al. Biosynthesis of gold nanoparticles assisted by lipopeptide biosurfactant derived from acinetobacter junii b6 and evaluation of its antibacterial and cytotoxic activities. BioNanoScience. 2020;10(4):899-908. https://doi.org/10.1007/s12668-020-00782-6.
37. Kasthuri J, Veerapandian S, Rajendiran N. Biological synthesis of silver and gold nanoparticles using apiin as reducing agent. Colloids and Surfaces B: Biointerfaces. 2009;68(1):55-60. https://doi.org/10.1016/j.colsurfb.2008.09.021.
38. Behera M, Ram S. Inquiring the mechanism of formation, encapsulation, and stabilization of gold nanoparticles by poly (vinyl pyrrolidone) molecules in 1-butanol. Applied Nanoscience. 2014;4:247-54. https://doi.org/10.1007/s13204-013-0198-9.
39. Kumar P, Aggarwal R. An overview of triple-negative breast cancer. Archives of gynecology and obstetrics. 2016;293:247-69. https://doi.org/10.1007/s00404-015-3859-y.
40. Murria R, Palanca S, de Juan I, Alenda C, Egoavil C, Segui FJ, et al. Immunohistochemical, genetic and epigenetic profiles of hereditary and triple negative breast cancers. Relevance in personalized medicine. Am J Cancer Res. 2015;5(7):2330-43.
41. Heimes AS, Schmidt M. Atezolizumab for the treatment of triple-negative breast cancer. Expert Opin Investig Drugs. 2019;28(1):1-5. https://doi.org/10.1080/13543784.2019.1552255.
42. Stringer-Reasor EM, May JE, Olariu E, Caterinicchia V, Li Y, Chen D, et al. An open-label, pilot study of veliparib and lapatinib in patients with metastatic, triple-negative breast cancer. Breast Cancer Res. 2021;23(1):30. https://doi.org/10.1186/s13058-021-01408-9.
43. Voorwerk L, Slagter M, Horlings HM, Sikorska K, van de Vijver KK, de Maaker M, et al. Immune induction strategies in metastatic triple-negative breast cancer to enhance the sensitivity to pd-1 blockade: The tonic trial. Nature medicine. 2019;25(6):920-8. https://doi.org/10.1038/s41591-019-0432-4.
44. Chen CY, Kao CL, Liu CM. The cancer prevention, anti-inflammatory and anti-oxidation of bioactive phytochemicals targeting the tlr4 signaling pathway. Int J Mol Sci. 2018;19(9):2729. https://doi.org/10.3390/ijms19092729.
45. Ranjan A, Ramachandran S, Gupta N, Kaushik I, Wright S, Srivastava S, et al. Role of phytochemicals in cancer prevention. Int J Mol Sci. 2019;20(20):4981. https://doi.org/10.3390/ijms20204981.
46. Rehman A, Ashfaq UA, Javed MR, Shahid F, Noor F, Aslam S. The screening of phytochemicals against ns5 polymerase to treat zika virus infection: Integrated computational based approach. Comb Chem High Throughput Screen. 2022;25(4):738-51. https://doi.org/10.2174/1386207324666210712091920.
47. Alam A, Haldar S, Thulasiram HV, Kumar R, Goyal M, Iqbal MS, et al. Novel anti-inflammatory activity of epoxyazadiradione against macrophage migration inhibitory factor: Inhibition of tautomerase and proinflammatory activities of macrophage migration inhibitory factor. J Biol Chem. 2012;287(29):24844-61. https://doi.org/10.1074/jbc.M112.341321.
48. Patil P, Patil S, Mane A, Verma S. Antidiabetic activity of alcoholic extract of neem (azadirachta indica) root bark. National Journal of Physiology, Pharmacy and Pharmacology. 2013;3(2):142. https://doi.org/10.5455/njppp.2013.3.134-138.
49. Shilpa G, Renjitha J, Saranga R, Sajin FK, Nair MS, Joy B, et al. Epoxyazadiradione purified from the azadirachta indica seed induced mitochondrial apoptosis and inhibition of nfkappab nuclear translocation in human cervical cancer cells. Phytother Res. 2017;31(12):1892-902. https://doi.org/10.1002/ptr.5932.
50. Aqil F, Munagala R, Jeyabalan J, Vadhanam MV. Bioavailability of phytochemicals and its enhancement by drug delivery systems. Cancer Lett. 2013;334(1):133-41. https://doi.org/10.1016/j.canlet.2013.02.032.
51. Mazurakova A, Koklesova L, Samec M, Kudela E, Kajo K, Skuciova V, et al. Anti-breast cancer effects of phytochemicals: Primary, secondary, and tertiary care. EPMA J. 2022;13(2):315-34. https://doi.org/10.1007/s13167-022-00277-2.
52. Mughees M, Wajid S. Herbal based polymeric nanoparticles as a therapeutic remedy for breast cancer. Anticancer Agents

Med Chem. 2021;21(4):433-44. https://doi.org/10.2174/1871520620666200619171616.
53. Dewhirst MW, Secomb TW. Transport of drugs from blood vessels to tumour tissue. Nat Rev Cancer. 2017;17(12):738-50. https://doi.org/10.1038/nrc.2017.93.
54. Gullotti E, Yeo Y. Extracellularly activated nanocarriers: A new paradigm of tumor targeted drug delivery. Mol Pharm. 2009;6(4):1041-51. https://doi.org/10.1021/mp900090z.
55. Zhen Z, Tang W, Chuang YJ, Todd T, Zhang W, Lin X, et al. Tumor vasculature targeted photodynamic therapy for enhanced delivery of nanoparticles. ACS Nano. 2014;8(6):6004-13. https://doi.org/10.1021/nn501134q.
56. Shabaninezhad M, Ramakrishna G. Theoretical investigation of size, shape, and aspect ratio effect on the lspr sensitivity of hollow-gold nanoshells. J Chem Phys. 2019;150(14):144116. https://doi.org/10.1063/1.5090885.
57. Creighton JA, Eadon DG. Ultraviolet–visible absorption spectra of the colloidal metallic elements. J Chem Soc Faraday Trans. 1991;87(24):3881-91. https://doi.org/10.1039/FT9918703881.
58. Kumar SS, Kumar CS, Mathiyarasu J, Phani KL. Stabilized gold nanoparticles by reduction using 3, 4-ethylenedioxythiophene-polystyrenesulfonate in aqueous solutions: Nanocomposite formation, stability, and application in catalysis. Langmuir. 2007;23(6):3401-8. https://doi.org/10.1021/la063150h.
59. Smitha SL, Philip D, Gopchandran KG. Green synthesis of gold nanoparticles using cinnamomum zeylanicum leaf broth. Spectrochim Acta A Mol Biomol Spectrosc. 2009;74(3):735-9. https://doi.org/10.1016/j.saa.2009.08.007.
60. Ahmad A, Syed F, Shah A, Khan Z, Tahir K, Khan AU, et al. Silver and gold nanoparticles from sargentodoxa cuneata: Synthesis, characterization and antileishmanial activity. Rsc Advances. 2015;5(90):73793-806. https://doi.org/10.1039/C5RA13206A.
61. Kabeerdass N, Kandasamy S, Albasher G, Alamri O, Alsultan N, Thangaswamy S, et al. Limonia acidissima leaf mediated gold nanoparticles synthesis and their antimicrobial and wound healing properties. Mater Lett. 2022;314:131893. https://doi.org/10.1016/j.matlet.2022.131893.
62. Haume K, Rosa S, Grellet S, Smialek MA, Butterworth KT, Solov'yov AV, et al. Gold nanoparticles for cancer radiotherapy: A review. Cancer Nanotechnol. 2016;7(1):8. https://doi.org/10.1186/s12645-016-0021-x.
63. Sztandera K, Gorzkiewicz M, Klajnert-Maculewicz B. Gold nanoparticles in cancer treatment. Mol Pharm. 2019;16(1):1-23. https://doi.org/10.1021/acs.molpharmaceut.8b00810.
64. Bhat AA, Thapa R, Afzal O, Agrawal N, Almalki WH, Kazmi I, et al. The pyroptotic role of *caspase-3*/gsdme signalling pathway among various cancer: A review. Int J Biol Macromol. 2023;242:124832. https://doi.org/10.1016/j.ijbiomac.2023.124832.
65. Zheng X, Chen W, Gong F, Chen Y, Chen E. The role and mechanism of pyroptosis and potential therapeutic targets in sepsis: A review. Front immunol. 2021; 12: 711939. 2021.

This work is licensed under a Creative Commons Attribution-Non Commercial 4.0 International License.